SCISPACE
formerly Typeset

Open access • Journal Article • DOI:10.1007/S00382-009-0614-8

Improvements in a half degree atmosphere/land version of the CCSM

— Source link

Peter R. Gent, Stephen Yeager, Richard Neale, Samuel Levis ...+1 more authors

Institutions: National Center for Atmospheric Research

Published on: 01 May 2010 - Climate Dynamics (Springer-Verlag)

Topics: Climate model, Climate oscillation, Arctic sea ice decline, Community Climate System Model and Global warming

Related papers:

- The Impact of Convection on ENSO: From a Delayed Oscillator to a Series of Events
- The Community Climate System Model Version 4
- The Community Climate System Model Version 3 (CCSM3)
- Global analyses of sea surface temperature, sea ice, and night marine air temperature since the late nineteenth century
- Improvements to the Community Land Model and their impact on the hydrological cycle

Share this paper:

View more about this paper here: https://typeset.io/papers/improvements-in-a-half-degree-atmosphere-land-version-of-the-58su4vmujd

Clim Dyn (2010) 34:819–833
DOI 10.1007/s00382-009-0614-8

Improvements in a half degree atmosphere/land version of the CCSM

Peter R. Gent · Stephen G. Yeager · Richard B. Neale · Samuel Levis · David A. Bailey

Received: 1 October 2008 / Accepted: 16 June 2009 / Published online: 1 July 2009
© Springer-Verlag 2009

Abstract A decadal climate projection between 1980 and 2030 using a nominal 0.5° resolution in the atmosphere and land components has been performed using the Community Climate System Model, version 3.5. The mean climate is compared to a companion simulation using a nominal 2° resolution in the atmosphere and land components. The increased atmosphere resolution has several benefits, and produces a significantly better mean climate. The maximum sea surface temperature biases in the major upwelling regions, including the West Coast of the USA, are reduced by more than 60%. Precipitation patterns are improved in the summer Asian monsoon, mostly due to the better resolved orography, and in the eastern tropical Pacific Ocean south of the equator. The improved precipitation patterns lead to better river flows in many rivers worldwide. The atmospheric circulation in the Arctic also improves, which leads to a better regional sea ice thickness distribution in the Arctic Ocean.

Keywords Climate · Projections · CCSM · Resolution

1 Introduction

Decadal climate projections and forecasts are starting to be made using climate models (Smith et al. 2007; Keenlyside et al. 2008). These papers have generated a lot of interest, because providing accurate, regional forecasts is a new, but very important, challenge for the climate modeling community. These decadal projections will be much shorter than the standard, multi-century climate projections, so most climate groups will do these decadal projections and forecasts with enhanced atmosphere resolution compared to the standard climate projections. It is naturally assumed that the higher atmosphere and land resolution will lead to considerably more accurate regional decadal climate projections than using the lower resolution version of the model. There are many papers showing improvements due to increased resolution in the atmosphere component, but the large majority run the atmosphere in isolation (May and Roeckner 2001; Brankovic and Gregory 2001; Pope and Stratton 2002; Kobayashi and Sugi 2004).

Hack et al. (2006) documents changes in the Community Climate System Model (CCSM) version 3 using the spectral atmosphere core at T85 and T42. The T85 version showed only minor improvements in the warm sea surface temperature (SST) biases in the upwelling regions, and in the double Intertropical Convergence Zone (ITCZ) bias in the tropical Pacific Ocean compared to the T42 version. (Bala et al. 2008) compares the T85 version of the CCSM 3 with a version using the new Lin-Rood finite volume core (Lin 2004) at 1° × 1.25°. Better surface wind stress and Arctic sea ice distribution are due to the new core, but the slightly reduced SST bias off the west coast of South America is likely due to the somewhat better atmosphere resolution in the finite volume core version. Very recently, (Navarra et al. 2008) describes significant improvements in their coupled model when the resolution in the atmosphere spectral core is increased from T30 to T106. They document improved tropical variability, especially in the Pacific Ocean, and improved coastal forcing along the west coast of South America. The El Nino—Southern Oscillation (ENSO) frequency peaks at 2 years in the T30 version, but the peak moves to longer periods in the T106 version more in line with observations. Improved ENSO characteristics

P. R. Gent (✉) · S. G. Yeager · R. B. Neale · S. Levis · D. A. Bailey
National Center for Atmospheric Research, Boulder, CO, USA
e-mail: gent@ucar.edu

due to increased atmosphere component resolution had previously been found by (Guilyardi et al. 2004). This change to improved ENSO periods longer than 2 years has also recently been achieved in the CCSM, but by changing two atmosphere component parameterizations, see Sect. 2 and Neale et al. (2008).

Normally, a new climate model version is defined by performing a several century pre-industrial control run and a twentieth century run. However, this would be very computationally expensive with the enhanced atmosphere resolution version. Instead, for the first run of this type using the CCSM, the higher resolution version was initialized by interpolating atmosphere and land data from a lower resolution twentieth century run at 1980, and integrating to 2030. Thus, this first run is a projection, and not a forecast, because no data is assimilated into any model component during this run. Most likely, the CCSM decadal predictions will initialize the ocean component to a representation of the true ocean state, and the best way to do this is a research problem that is being addressed at the present time. However, runs without ocean initialization of the type described in this paper will be very useful both to provide initial conditions for the other model components in the decadal forecasts, and for comparisons to determine whether it is important to initialize the ocean or not. This paper does not report on the ocean initialization methods being tried in the CCSM, but has the more modest goal of documenting the mean climate improvements seen in the enhanced atmosphere resolution version compared to the standard atmosphere resolution version.

The model used is the CCSM version 3.5, which is an interim version of the CCSM assembled in October 2007. The next released version, CCSM 4, will actually be used to make these decadal climate projections and predictions when it is ready. Even though CCSM 3.5 is only an interim version, the results presented in this paper are robust enough that they will almost certainly also apply to the CCSM 4. The reason is that many improvements are due to the much better resolved orography in the higher resolution run. The changes between versions CCSM 3 and CCSM 3.5 are documented in Sect. 2. One of the major changes is that the atmosphere component has switched from a spectral to a finite volume dynamical core. The standard atmosphere resolution in the new finite volume core is 192×72 points, which corresponds to $1.9° \times 2.5°$; henceforth called 2°. The higher resolution uses four times as many points in both horizontal directions, giving an atmosphere resolution of $0.47° \times 0.63°$, henceforth called 0.5°. These are also the resolutions of the land component in the two runs. In both runs, the ocean and sea ice components use the standard CCSM 1° resolution, which is defined in Sect. 2. Several aspects of the mean climates between 1985 and 2000 from the two different resolution runs are compared in Sect. 3, and Sect. 4 contains the conclusions and discussion.

2 The CCSM 3.5 and integrations

The CCSM is a general circulation climate model that couples atmosphere, land, ocean, and sea ice components. An overview and a description of the CCSM version 3 present day climate simulation using T85 (1.4°) atmosphere and land resolution, and a nominal 1° ocean and sea ice resolution are given in (Collins et al. 2006). Version 3.5 is an interim version on the way to the next release of the CCSM. It has numerous changes and improvements to version 3, which will be briefly documented here.

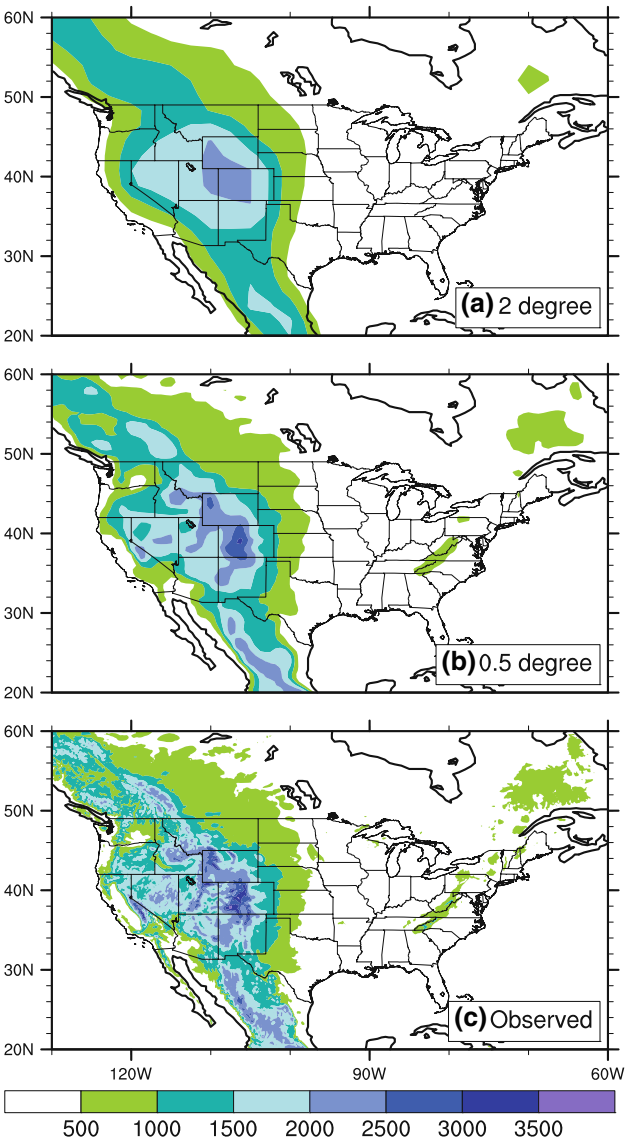

Fig. 1 North America orographic height in meter at (**a**) 2°, (**b**) 0.5°, and (**c**) 10-min resolution

The core of the Community Atmosphere Model (CAM) version 3.5, changed from the spectral core used in CAM 3 to the Lin-Rood finite volume core (Lin 2004). Changes were made to the deep convection scheme by including the effects of deep convection in the momentum equation (Richter and Rasch 2008), and using a dilute, rather than an undilute, approximation in the plume calculation. These changes resulted in a major improvement in the simulation of ENSO in CCSM 3.5, which is documented in (Neale et al. 2008). In CCSM 3, the ENSO frequency was dominated by variability at 2 years, whereas in 3.5 there is virtually no power at 2 years, and the power is between 3 and 6 years. In addition, the mean precipitation and double ITCZ biases in the western tropical Pacific Ocean were reduced, but certainly not eliminated. A freeze-dry modification was added to the low cloud parameterization, which had the effect of reducing the amount of low cloud in the Arctic region. The horizontal resolution in the two runs is given above, and there are 26 levels in the vertical in both versions of CAM.

Moving from 2° to 0.5° resolution in CAM 3.5 begins to resolve a number of important topographic features over the United States, see Fig. 1. In the western US, the single low maximum of 2,300 m over the whole Rocky Mountains at 2° is replaced by a more localized mountain maximum of over 3,000 m in western Colorado, in addition to the distinct maxima of the Wyoming range, the Utah Wasatch range, the Idaho Salmon River range and the southern Rockies of New Mexico. Further west and north, the Cascades and the Sierra Nevadas become distinct and play a greater role in directing the prevailing onshore flow and shaping the model climate. In the Eastern US, the Appalachians now become a distinct feature reaching well over 500 m.

There have also been a number of changes to the ocean component of CCSM 3.5. The eddy parameterization transition near the surface has been modified (Danabasoglu et al. 2008), and the isopycnal diffusivity is now a function of space and time (Danabasoglu and Marshall 2007). The anisotropic horizontal viscosity scheme has been changed, and the viscosity is now substantially smaller near the equator and the western boundaries of ocean basins (Jochum et al. 2008). The vertical mixing terms now have a term that is proportional to the tidal energy, and the advection scheme has been changed from the third-order upwind scheme to a flux-limited scheme that is much less diffusive. The nominal 1° grid uses spherical coordinates in the southern hemisphere, but in the northern hemisphere the pole is displaced into Greenland at 80°N, 40°W. The horizontal grid has 320 × 384 points, and the resolution is a uniform 1.11° in the zonal direction. In the southern hemisphere, the meridional resolution is 0.27° at the equator, gradually increasing to 0.54° at 33°S, and is constant at higher latitudes. There are now 60 levels in the vertical in the ocean component, as opposed to 40 in CCSM 3, with improved resolution in the upper ocean.

The Community Land Model (CLM), version 3.5 is documented in (Oleson et al. 2008; Stockli et al. 2008). There were changes to several parts of the model hydrology, such as the surface runoff, the groundwater scheme, the frozen soil scheme, and a soil evaporation resistance was added. Other new features are a revised canopy integration, canopy interception scaling, and a plant functional type dependency on the soil moisture stress function. CLM 3.5 has a much improved representation of evapotranspiration and the annual cycle of water storage, for example. The CLM is fundamentally a column model, and so simulates processes that are independent of horizontal resolution. However, it uses the same horizontal grid as the atmosphere component, so the CLM forcings change with changing atmosphere resolution.

The sea ice component in CCSM 3.5 moved to the Community Ice Code (CICE), version 4.0 as its base code, which is maintained at the Los Alamos National Laboratory, see http://climate.lanl.gov/source/projects/climate/Models/CICE/cicedoc.pdf. This brought in improved treatments of ice ridging and snow on top of the ice. In addition, a much improved radiative transfer scheme was implemented (Briegleb and Light 2007), and a new melt pond parameterization was also included. It uses five thickness categories for ice, as well as a snow layer, and is solved on the same horizontal grid as the ocean component.

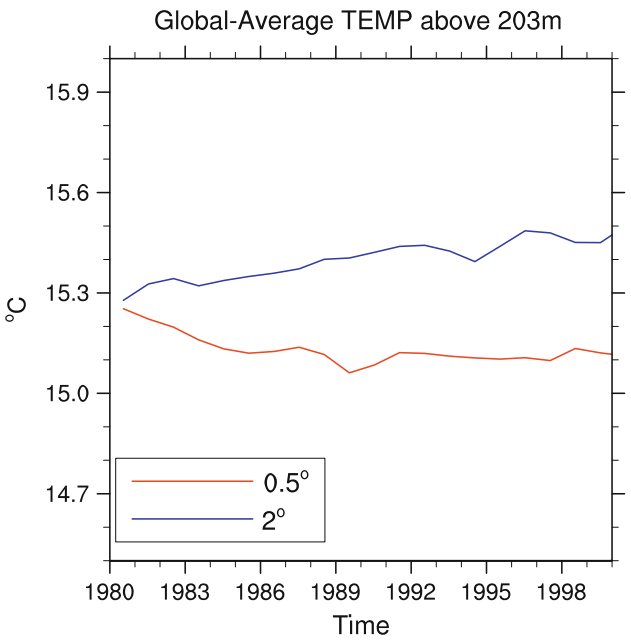

Fig. 2 Globally-averaged ocean temperature above 203 m between 1980 and 2000 from the 2° and 0.5° runs

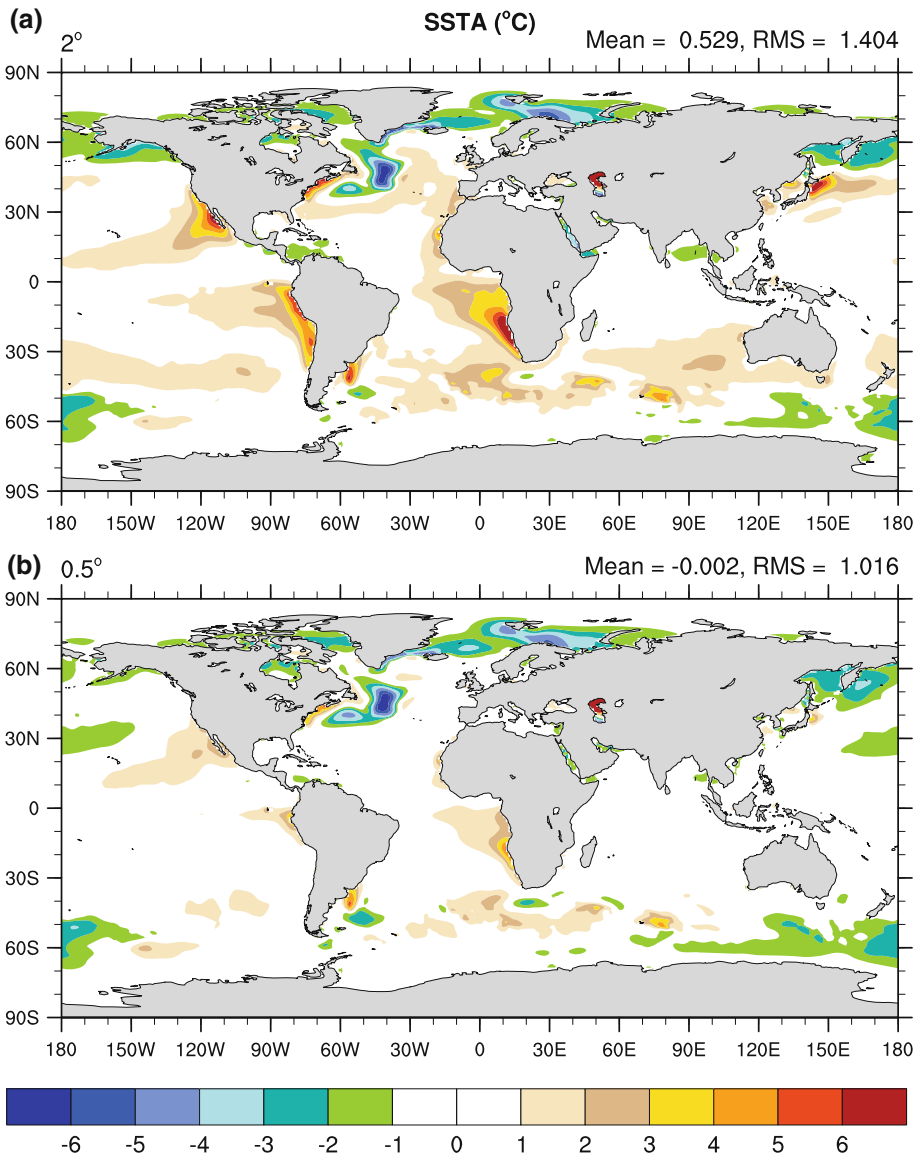

Fig. 3 Difference between the SST in (**a**) 2° run, and (**b**) 0.5° run and observations (Levitus et al. 1998; Steele et al. 2001)

First, a 2° atmosphere and land, 1° ocean and sea ice 1870 Control run was integrated for 260 years, which had a good top of the atmosphere balance of -0.12 W/m^2. The 2° run was branched from year 123 of the Control run, and was integrated from 1870 to 2030. The greenhouse gas forcing was taken from observations between 1870 and 2000, and then followed the Special Report on Emissions Scenarios A1B future scenario. Additional forcings are the levels of dust, sea salt, and carbonaceous and sulphate aerosols. These aerosol levels are based on a historical reconstruction run using the CCSM chemistry component, and then projected forward for the period 2000–2030. The solar forcing was held constant at 1,365 W/m^2, and no volcanic forcing was applied to the run. The initial condition for the 0.5° run was taken from 1 January 1980 of the 2° run. The atmosphere and land fields were interpolated onto the 0.5° grid, and the ocean and sea ice fields were used without modification. The 0.5° run was integrated from 1980 to 2030, and was forced in exactly the same way as the 2° run. The factor of 16 times more grid points in the atmosphere and land components, but the same number in the ocean and sea ice components, means the 0.5° run takes about 12 times the computational resource of the 2° run.

3 Comparison of mean climates

This section will compare several aspects of the 2° and 0.5° run climates averaged between the beginning of 1985 and 2000, and observations representing the end of the twentieth century. The rationale for averaging between 1985 and 2000 is the following. The 0.5° run will obviously have a period of adjustment to its own climatology from that of the 2° run. Figure 2 shows the globally averaged ocean temperature

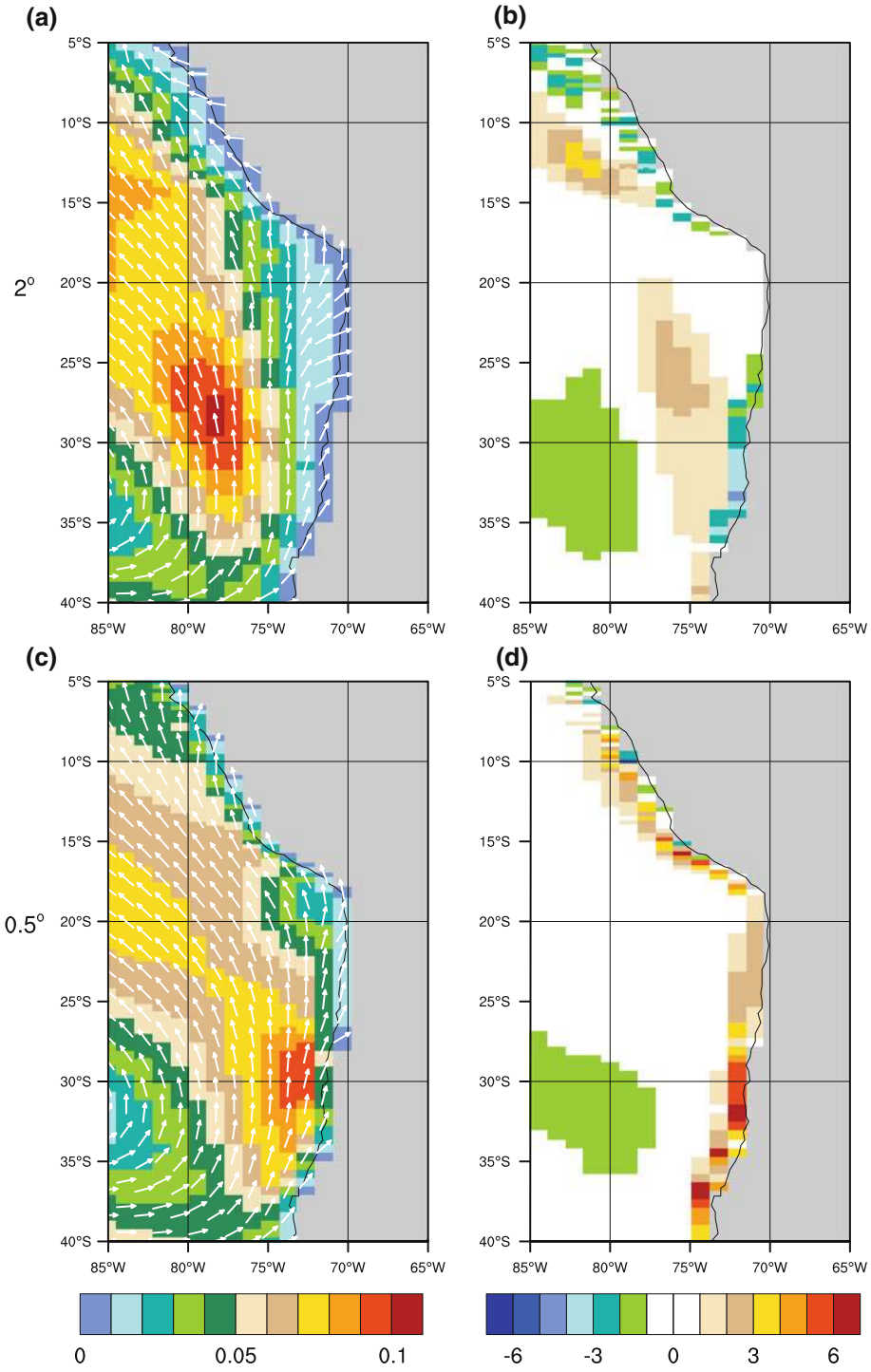

Fig. 4 **a** Wind stress magnitude (N m^{-2}) and direction. **b** Vertical velocity at 100 m depth 10^{-6} m/s from the 2° run along the west coast of South America. **c**, **d** The same from the 0.5° run

between the surface and 203 m depth between 1980 and 2000 from the two runs. It shows that most of the adjustment in the upper 200 m of the ocean occurs in the first 5 years, and the adjustment to the new 0.5° climatology is almost complete after 10 years. Adjustment to the new Arctic Ocean sea ice thickness distribution in the 0.5° run also takes 5–10 years, and the adjustment in the atmosphere and land components is faster than this. Thus, the choice was made to start the averaging in 1985, rather than in 1990, in order to have a longer averaging period, given that most of the upper ocean adjustment had occurred by then.

3.1 The upper ocean simulation

Figure 3 shows the difference between the SST in the two runs and a climatology from (Levitus et al. 1998) data and

(Steele et al. 2001) data in the Arctic. Figure 3a shows the average SST bias over 1985–2000 for the 2° run, which is very typical of errors found in previous CCSM runs at this resolution. The largest positive SST errors of more than 6°C are in the three major upwelling regions off the west coasts of North and South America and off Southern Africa. Figure 3b from the 0.5° run shows that the SST errors in the upwelling regions are very significantly reduced. The maximum errors are reduced by more than 60% off North and South America, and the area of biases larger than 2°C is very significantly reduced in all three upwelling regions.

The 0.5° atmospheric resolution resolves orography much better, see Fig. 1, and this allows the strongest surface winds in the upwelling regions to be located much nearer the coasts. This immediately increases the coastal upwelling, which reduces the SST. The colder SST and surface atmospheric temperature allows more stratus clouds to form, which shield the sunlight reaching the ocean, and further reduce the SST. Thus, the positive feedbacks between the ocean and atmosphere that led to the large positive SST errors are strongly alleviated in the 0.5° run. The evidence for this sequence of events is in Fig. 4, which shows the surface wind stress magnitude and direction, and the vertical velocity at 100 m depth in the ocean from the two runs along the west coast of South America. Figure 4(a, c) shows that the maximum wind stress is located much closer to the coast in the 0.5° run, and is directed more parallel to the coast. This is more favorable for upwelling, and Fig. 4(b, d) shows that the vertical velocity at 100 m along the coast is significantly stronger in the 0.5° run. The CCSM project has spent much effort trying to reduce these upwelling region SST biases in previous model versions by changing atmosphere and ocean parameterizations. This has never worked satisfactorily, and the only known way to reduce these biases is to use much finer resolution in the atmosphere.

Figure 3 shows that the globally averaged SST bias in the 0.5° run is reduced by more than 0.5°C, and is very small when compared to the observations. One reason for this reduction is that the colder surface water in the upwelling regions is advected out into the eastern parts of the North and South Pacific Ocean and the South Atlantic Ocean. This effect has been clearly documented in Sect. 5 of Large and Danabasoglu (2006). They ran a series of experiments using the CCSM 3 where the ocean temperature and salinity were very strongly restored to observations in these three upwelling regions between the surface and 500 m depth. Their Fig. 7 shows that the SST, sea surface salinity (SSS) and precipitation biases were significantly reduced throughout the eastern parts of the three ocean basins. The same effect is occurring in the 0.5° run, although to a lesser degree because the SST errors in the upwelling regions are strongly reduced, but not completely eliminated, as they were in the (Large and Danabasoglu 2006) experiments.

The (Large and Danabasoglu 2006) experiments also show that restoring the SST to observations in the South America upwelling region greatly improves another very persistent CCSM bias, which is the annual cycle of SST along the equator in the eastern Pacific Ocean. Thus, we would expect this bias to be improved in the 0.5° run. Figure 5 shows the SST averaged between 0.5°N and S across the Pacific Ocean from the two runs and the (Smith and Reynolds 1998) climatology, and the annual cycle of the SST anomaly at 262.5°E. The 0.5° run SST is a little warmer across much of the equatorial Pacific, and both are warmer than the observations, especially near the ocean boundaries. The observations in Fig. 5b show a very dominant annual cycle in the SST anomaly at 262.5°E, which is not captured at all in the 2° run where there is a dominant semiannual cycle. The 0.5° run shows improvement such that the dominant cycle is annual rather than semiannual. However, there is still plenty of room to improve both the amplitude and phase of the SST annual cycle along the equator. This bias would be improved further if the SST errors in the upwelling region off South America in the 0.5° run were eliminated.

Figure 3a also shows there are large SST errors in the North Atlantic, where the path of the Gulf Stream is too far south, and in the region of the Kuroshio separation, which

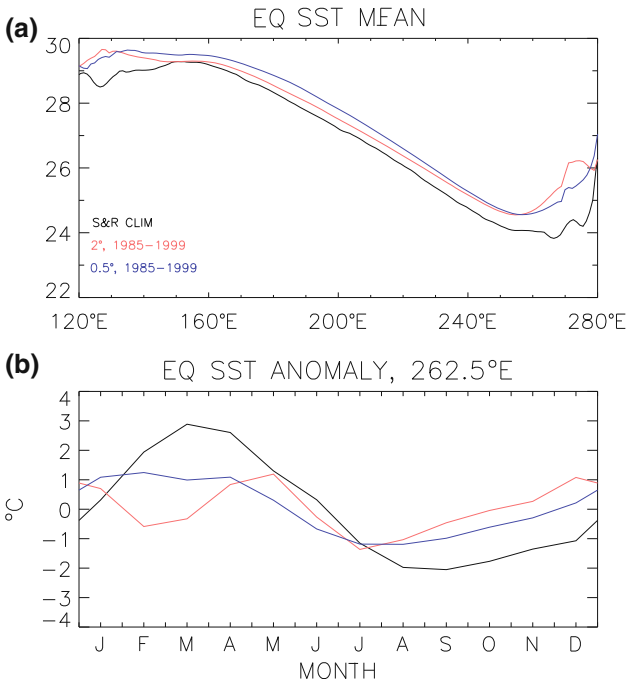

Fig. 5 **a** Mean equatorial SST across the Pacific from the 2° and 0.5° runs and observations (Smith and Reynolds 1998). **b** Mean monthly SST anomalies at 262.5°E

is too far north off Japan. In the 0.5° run, shown in Fig. 3b, the error in the North Atlantic remains, but the Kuroshio separation is improved and the SST bias reduced significantly, again probably due to improved atmospheric winds. The SST improvements in the 0.5° run are reflected in reduced temperature biases over the upper ocean down to about 400 m, but below that depth the biases are comparable in the two runs.

Figure 6 shows the difference between the SSS in the two runs and the Levitus et al. (1998) and Steele et al. (2001) climatology, and shows there is also a marked improvement in SSS in the 0.5° run. Fresh biases in all three upwelling zones and adjacent ocean basins are significantly reduced. In addition, the salty biases in the tropical Atlantic, Indian and central Pacific Oceans are also strongly reduced. However, large biases remain in the Arctic Ocean compared to the (Steele et al. 2001) climatology. The improvement in SSS is more difficult to analyse than SST because it depends on the atmospheric precipitation patterns and on the river runoff from the land component, which are analysed below.

3.2 The atmosphere simulation

The atmosphere simulation has a number of improvements on both the global and regional scale at 0.5° resolution. Globally, the ocean surface pressure distribution is much improved in the midlatitudes due to the enhanced baroclinicity at higher resolution. (Williamson 2008) has recently shown that a horizontal resolution much higher than 2° is required with the finite volume core in order to obtain convergence in the strength of baroclinic eddies.

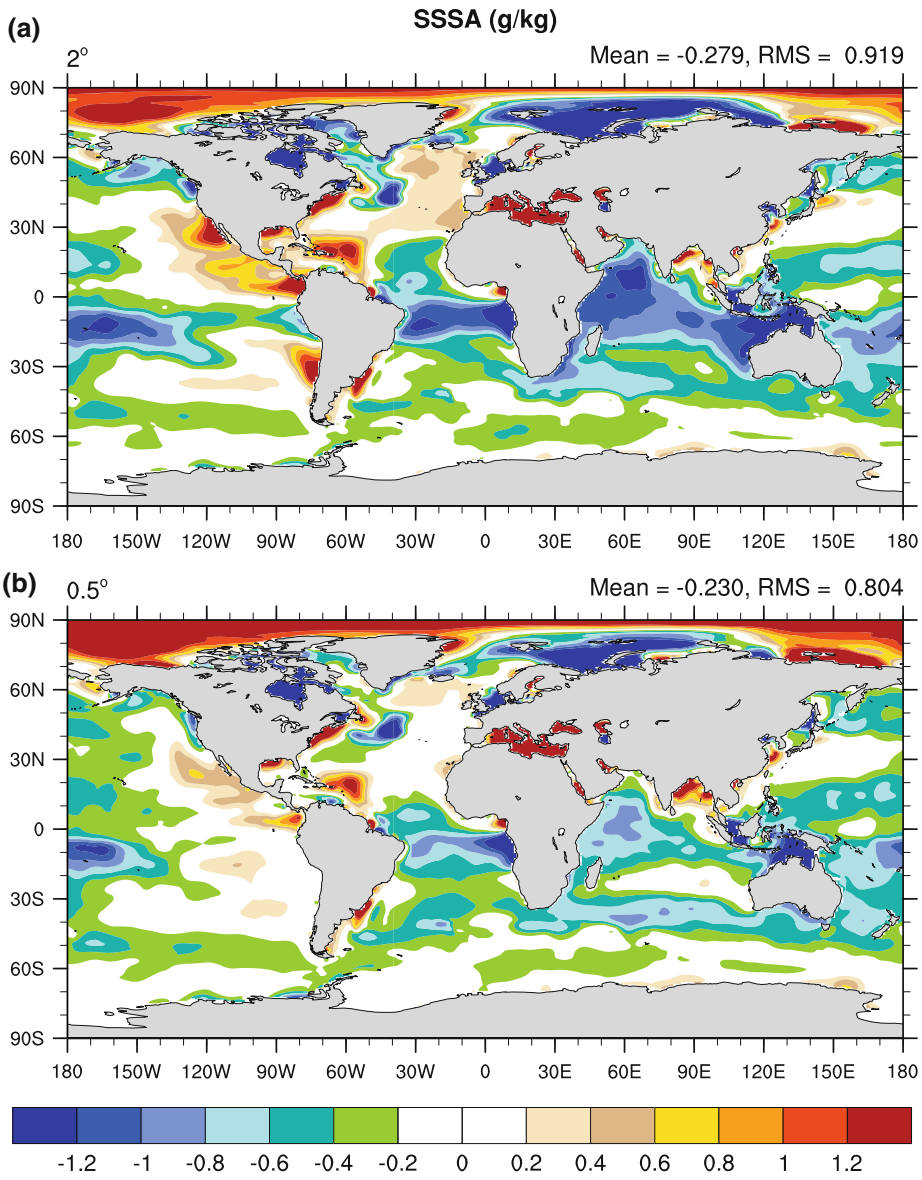

Fig. 6 Same as Fig. 3, but for sea surface salinity

Precipitation changes in the US between the two runs are related to the better resolved orographic features shown in Fig. 1. Figure 7(a, b) shows the winter-time precipitation biases in the 2° and 0.5° runs from the Willmott and Matsuura (2001) observations, which are shown in Fig. 7c. In the southeast the 2° run has a dry bias of nearly 3 mm/day which, due to the uplift of the flow by the better resolved Appalachian chain in the 0.5° run, is reduced in areal extent and size to less than 2 mm/day. In the interior West, orography related precipitation features are better represented in the 0.5° run, but there is still a general large-scale wet bias of at least 1 mm/day. The precipitation distribution is significantly improved in the rain shadow of eastern Washington and south-west Canada, with much reduced wet biases as the flow is directed more southwards by better resolved orography. However, California has a significant wet bias in the 0.5° run due to this flow redirection and greater uplift from the Sierra Nevada range.

Figure 8 shows the summer-time precipitation biases in the same format as Fig. 7. Precipitation in the 2° run is excessive in the central high-plains region, with a bias of over 5 mm/day representing a 200% excess compared to observations. In the 0.5° run, this bias is reduced by about

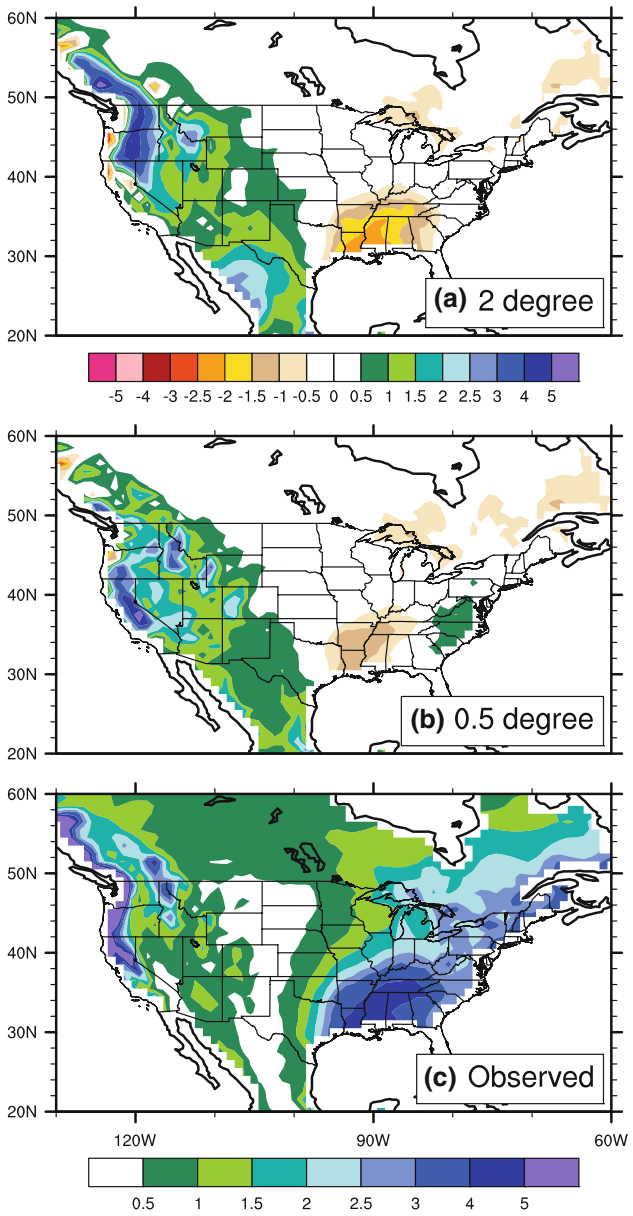

Fig. 7 DJF US precipitation biases (mm/day) for (**a**) 2° and (**b**) 0.5° runs compared to observations (Willmott and Matsuura 2001) which are shown in panel (**c**)

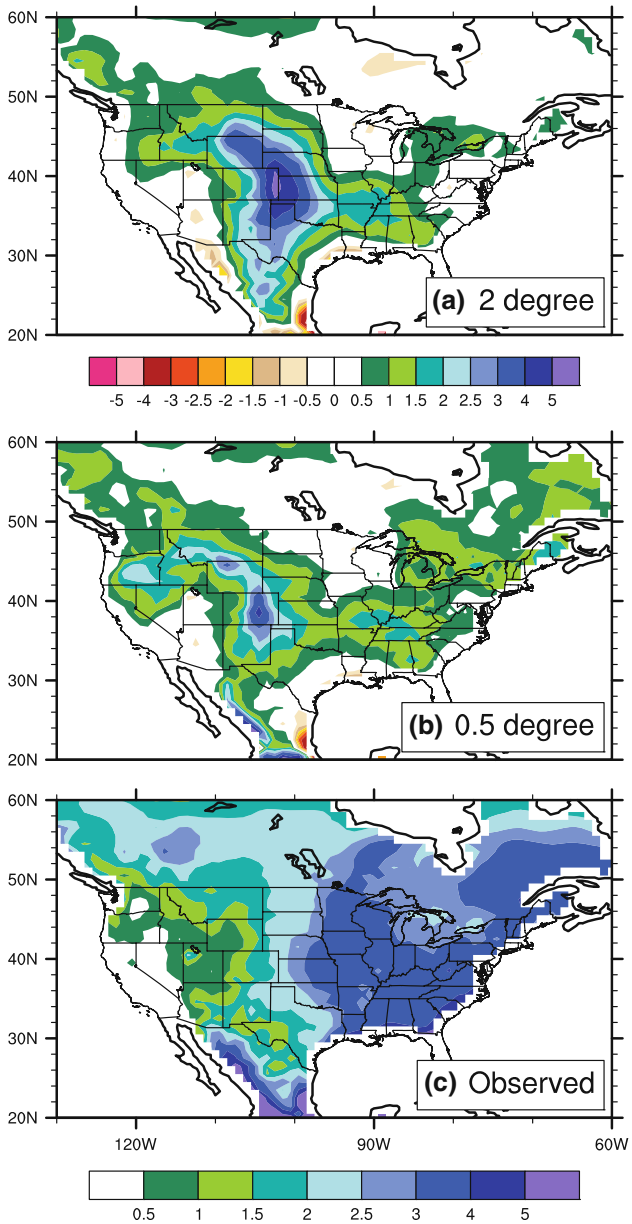

Fig. 8 Same as Fig. 7, but for JJA

half in terms of both magnitude and areal extent. The error occurs during part of the North American summer monsoon period, and involves subtle differences between the moisture supply and large-scale forcing. The largest precipitation errors are co-located with significant mid-tropospheric centers of convergence. Although the Great Plains low-level jet and its moisture transport are well represented in both runs, the configuration of the orography is such that the jet experiences large mechanical uplift in the 2° run, but much smaller uplift in the 0.5° run. In reality, there is minimal uplift of the observed jet as the flow is better constrained to be up against the Rocky Mountains by compensating weak subsidence from the major monsoon circulation.

Elsewhere, the 0.5° run shows significant improvement in the Asian summer monsoon due to the more realistic interaction with orography. Figure 9 shows the summer-time precipitation and orography greater than 400 m in this region from the 2° and 0.5° runs, and the observational estimates from Tropical Rainfall Measuring Mission (TRMM) data. Figure 9a shows that the 2° run poorly simulates the close proximity of the precipitation features to the orographic features, such that the zonal distribution of precipitation varies unrealistically smoothly from the Arabian Sea through to the west Pacific. The 0.5° run improves on this significantly, because the precipitation features are tightly bound to the better resolved mountain chains of the Indian Western Ghats, and the mountains of Burma and Cambodia. Some of these features, such as the Western Ghats mountains, extend for only 100 km in the east–west direction, and so are severely under resolved with 2° resolution. In these regions, the moisture laden low-level westerly flow ascends over the better resolved orographic features, but also strongly descends with low water loading on the leeward side of the ranges thus reproducing the observed rain shadow regions. Figure 10 shows this dynamically where the 700 hPa zonal flow errors compared to the ERA40 reanalysis are much improved in the 0.5° run, leading to more localized ascent over the orography and descent to the east of India suppressing precipitation. Further

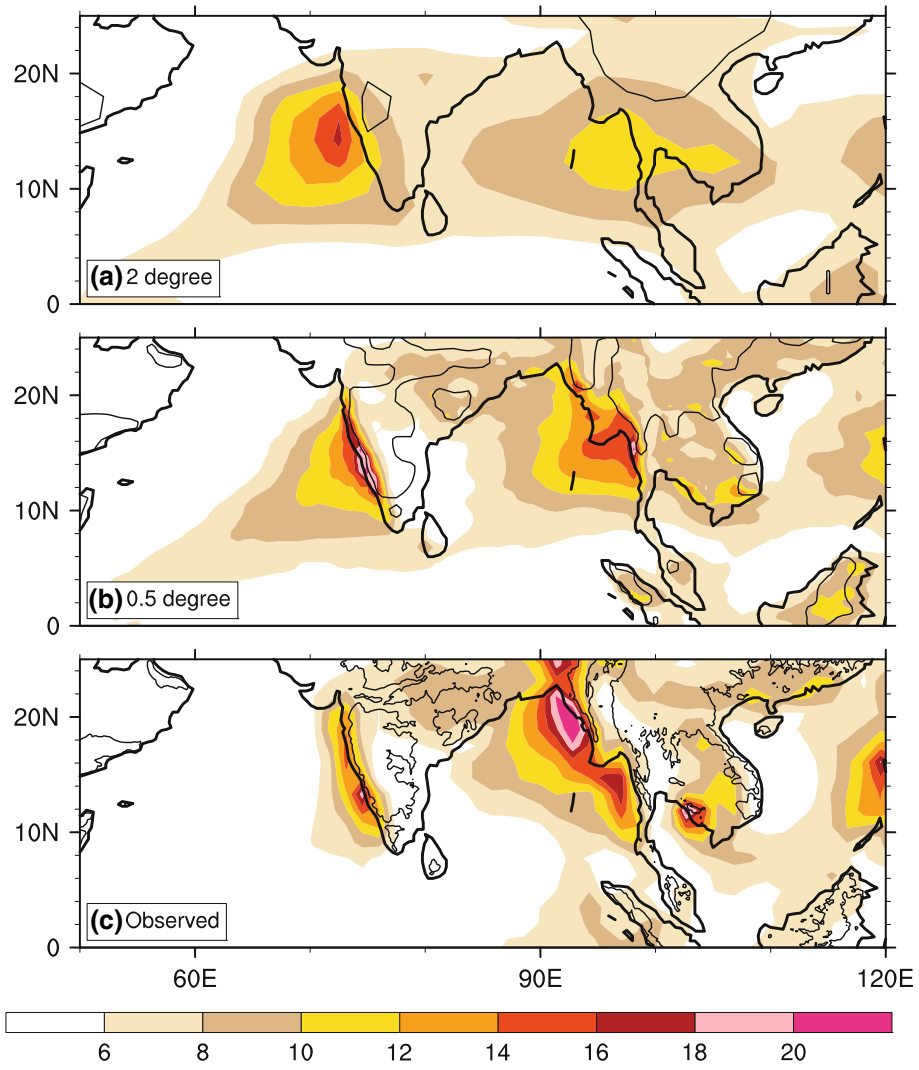

Fig. 9 Asian monsoon JJA precipitation (mm/day) for (**a**) 2°, (**b**) 0.5° and (**c**) observations (TRMM). The resolved orography higher than 400 m is shown with the single solid contour over land

east, a similar pattern of improvement is seen in the intense precipitation maximum and rain shadow of the South-East Asian component of the monsoon.

Higher horizontal resolution also improves the simulation of the longstanding double-ITCZ problem in the eastern Pacific Ocean. Figure 11 shows the DJF precipitation and the 925 hPa convergence in this region from the 2° and 0.5° runs, and the observational estimates from TRMM and ERA40 reanalysis. It shows that the precipitation maximum flips erroneously to the southern hemisphere during DJF in the 2° run, but the 0.5° run is able to maintain its observed position north of the equator. This is a consistent response to the low-level troposphere flow convergence line being maintained north of the equator during this time, in response to the much colder SSTs in the eastern Pacific south of the equator in the 0.5° run. In the 2° run, the warmer SSTs in this region allow the erroneous convection and associated convergence to be south of the equator. It is also clear from Fig. 11b that the double-ITCZ problem in the East Pacific has not been eliminated in the 0.5° run, which still has erroneous precipitation south of the equator in DJF. This reduction in precipitation south of the equator is consistent with the results from the CCSM 3 experiments of Large and Danabasoglu (2006) mentioned above. It should also be noted that the higher resolution of the 0.5° run does not improve at all the double-ITCZ bias in the western Pacific Ocean. This bias was even larger in the CCSM 3; it's magnitude is somewhat reduced in these CCSM 3.5 runs because of the improved parameterizations in CAM 3.5, but it certainly has not been eliminated.

3.3 The land simulation

Increasing horizontal resolution in the CLM forced by prescribed atmosphere data might improve the model

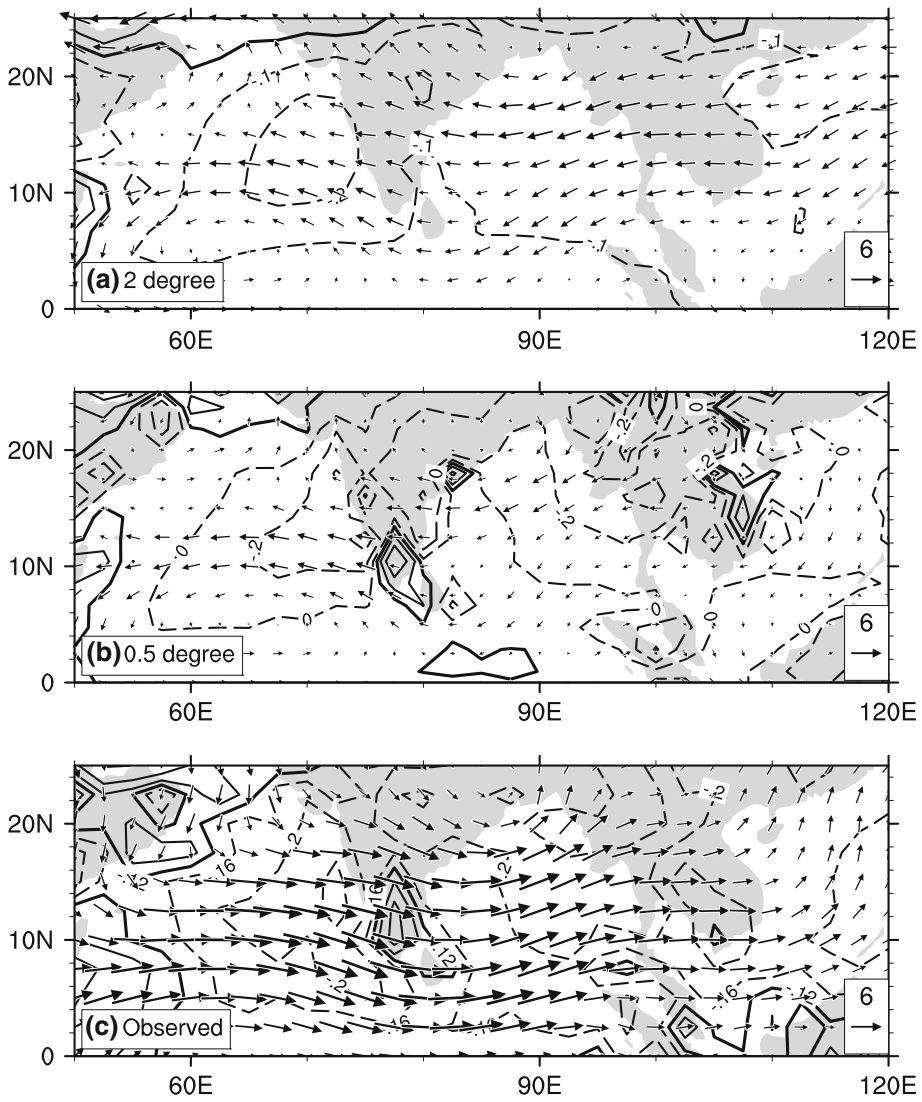

Fig. 10 Asian monsoon JJA 700 hPa wind errors (vectors, m/s) and vertical velocity (contours, hPa/h) for (**a**) 2°, (**b**) 0.5° and (**c**) observations (ERA40, where full field winds are shown)

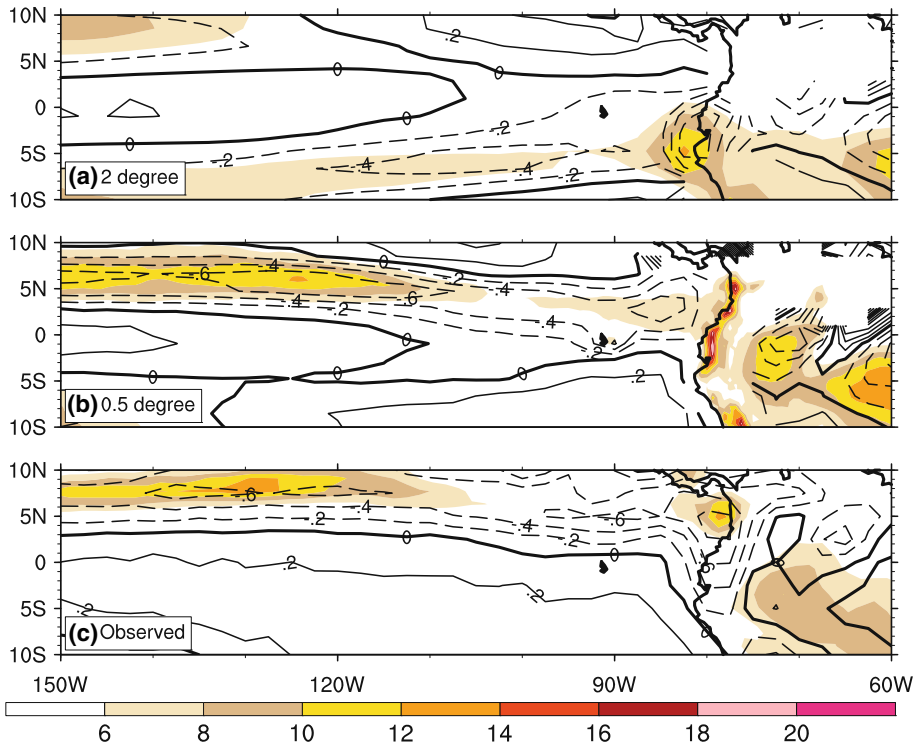

Fig. 11 East Pacific DJF ITCZ precipitation (mm/day) and 925 hPa convergence (10^5 s^{-1}) for (**a**) 2° run, (**b**) 0.5° run, and (**c**) observations (TRMM precipitation; ERA40 reanalysis divergence)

results, especially near discontinuities such as along rain/snow lines, or in areas with steep gradients in vegetation or other surface characteristics. In simulations where the CLM is coupled, such improvements influence the results through feedbacks, but CLM's changed effect on the climate is generally second order relative to the simulated changes in temperature, precipitation, and clouds originating in the atmosphere. CLM's river transport module (RTM) (Branstetter and Erickson 2003), is an integrator of near surface processes and can be used to assess basin-wide improvements in the coupled simulation. The RTM provides a one-way connection between the land and ocean, with potential effects on ocean circulation. The RTM operates on a 0.5° grid regardless of the chosen CLM resolution.

The RTM results generally improve in the 0.5° run relative to the 2° run. There are notable changes in discharge between the two runs for some of the largest rivers in the world, which are shown in Fig. 12 along with observational estimates from (Dai and Trenberth 2002). The flow of the Amazon improves by increasing year round in the 0.5° run. The flows of the Brahmaputra, Ganges, and Changjiang also improve by decreasing specifically from July to January. The Orinoco and Parana do not improve, and rather switch from underestimated in most months in the 2° run to overestimated in most months in the 0.5° run. The Mississippi River improves from August to October by decreasing in the 0.5° run, but is more underestimated now during the rest of the year. Smaller North American rivers (not shown), such as the Rio Grande, Mackenzie, Yukon, and Fraser Rivers improve by decreasing in volume, whereas the Colorado and St. Lawrence Rivers improve a little by increasing in volume. However, discharge from the Nelson and Sacramento Rivers deteriorates in the 0.5° run by decreasing and increasing, respectively.

Figure 13 shows that the cumulative annual discharge into the Atlantic Ocean improves very markedly in the 0.5° run compared to the (Dai and Trenberth 2002) observations. This is mostly due to the substantial increase in Amazon River flow that enters the Atlantic at the equator. However, the annual discharge into the global oceans, which is underestimated in most months in the 2° run, is overestimated in most months in the 0.5° run. This switch is due to a large increase in 0–10°S discharge into the Pacific Ocean, because the flow in the Sepik and Purari Rivers in Papua New Guinea doubles. For the world's fifty largest rivers, the 2° run has better flow at 19 gauge stations, and the 0.5° run has better flow at 31 stations. The tendency for improved river flows in the 0.5° run strongly suggests an improved simulation of the near surface energy and hydrological cycles. Oleson et al. (2008) documents these aspects of CLM 3.5 in detail.

Snow cover fraction, snow water equivalent, and snow depth show a mix of improved and degraded results in the 0.5° run. The most notable large scale result is that snow fraction underestimation in the 2° run has improved in the 0.5° run along a latitudinal swath from eastern Europe to about 70°E in winter, spring, and fall, suggesting better

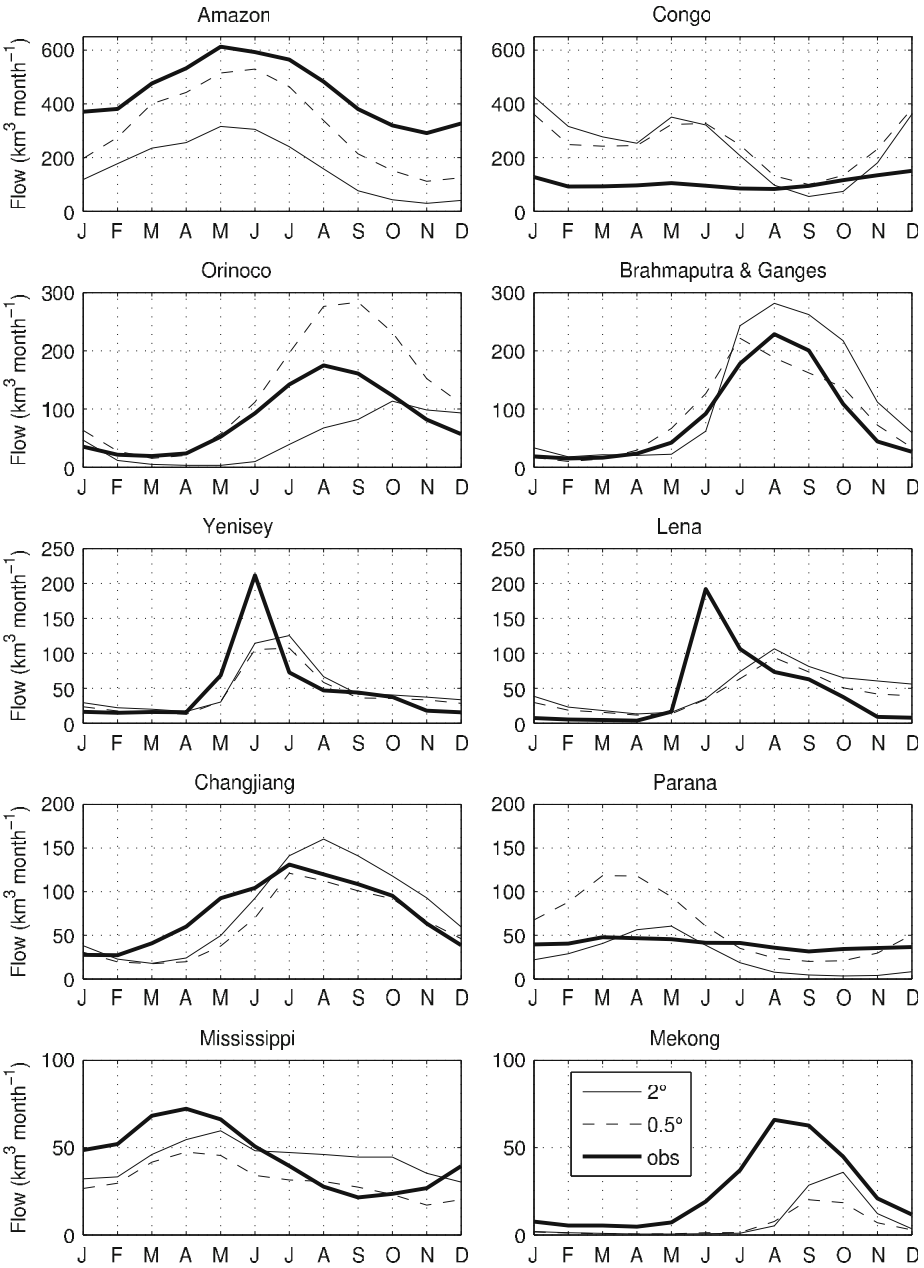

Fig. 12 Annual cycle of flow in 10 major rivers from the 2° and 0.5° runs and observations (Dai and Trenberth 2002)

representation of the rain/snow line. Focusing on North America, there are various levels of improvement in snow cover fraction, snow water equivalent, and snow depth in northwestern, central, and eastern Canada, as well as in western and eastern USA. Generally, more regions are improved than degraded with respect to the snow simulation.

3.4 The arctic sea ice simulation

There are some regional improvements in the Arctic sea ice thickness simulation in the 0.5° run compared to the 2° run, which is shown in Fig. 14 averaged over 1985–2000 from the two runs. The sea ice is too thick in the 2° run compared to the best observational estimates in the Siberian Sea region off eastern Russia, and is reduced by about 1 m in the 0.5° run. The area of reduced ice thickness extends away from the Russian coast into the central Arctic Ocean, but then the difference changes sign, and the ice is thicker along the Canadian coast in the 0.5° run. The ice thickness and extent in the western Arctic are generally improved because the 0.5° resolution atmosphere simulates the anticyclonic Beaufort Gyre circulation in a better location (not shown). It is moved towards North America, which has two positive effects. First, sea ice is transported away from the Russian coast in the 0.5° run rather than into the Siberian Sea in the 2° run, so that the sea ice is much thinner in the Siberian Sea in the 0.5° run. Second, the sea

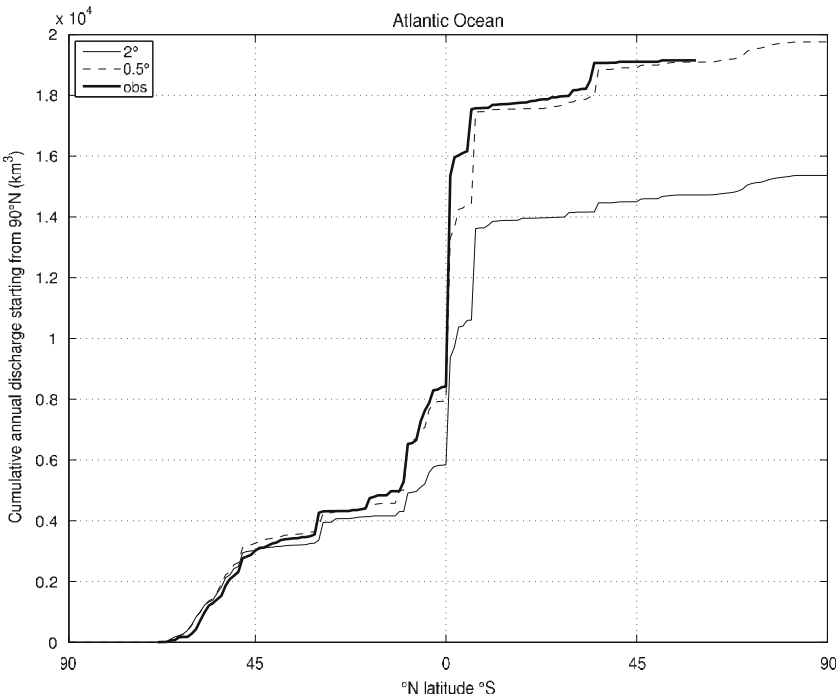

Fig. 13 Annual river discharge into the Atlantic Ocean as a function of latitude from the 2° and 0.5° runs and observations (Dai and Trenberth 2002)

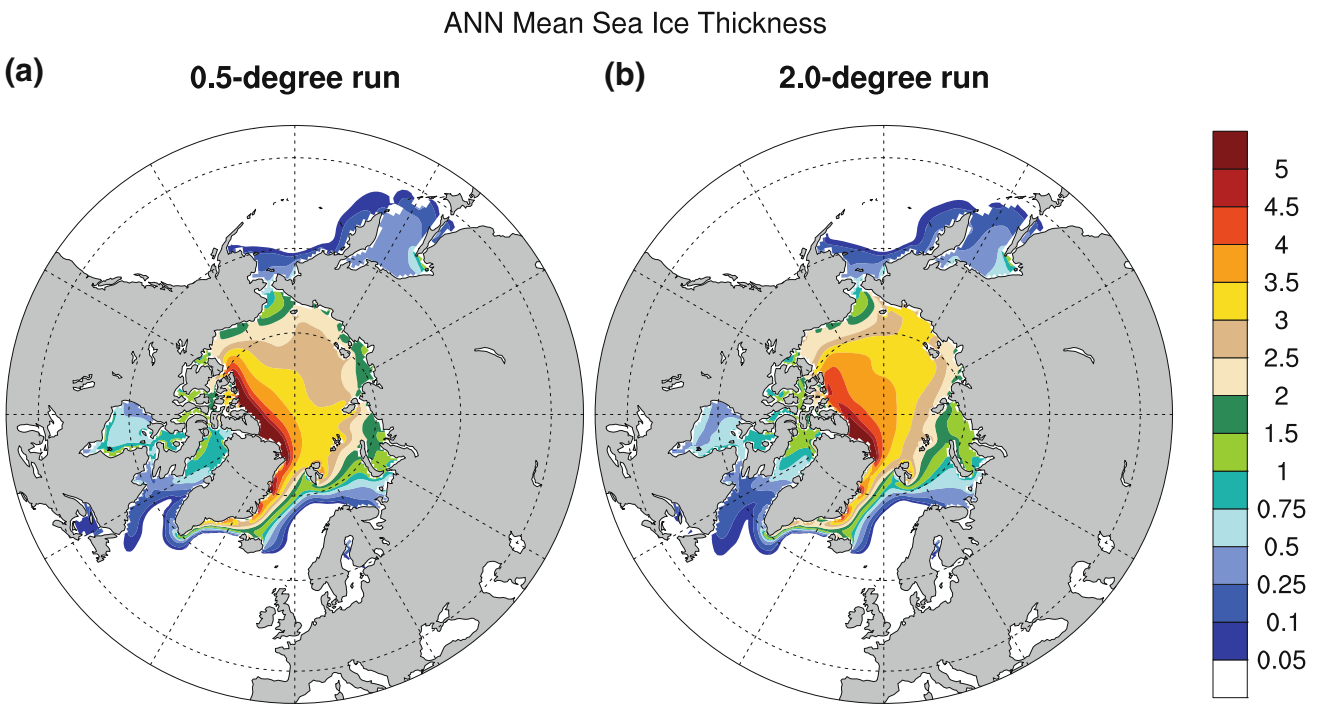

Fig. 14 Annual mean Arctic sea ice thickness in meter from (**a**) 0.5° run, and (**b**) 2° run

ice is pushed more towards the Canadian Archipelago where it builds up thicker ice in better agreement with observations. The overall improvement in sea ice thickness is due to the better Arctic circulation, and results in a reduced ice velocity through Fram Strait in the 0.5° run.

The Labrador Sea is an area where it is extremely difficult to simulate accurately the sea ice extent because of the very strong atmosphere–ice–ocean interaction in this region. The exact position of the ice edge in the Labrador Sea exhibits considerable annual and decadal variability in observations and in the CCSM. In the same integration there can be decades with too much ice, followed by decades with too little ice compared to the observed mean. Figure 15 shows the time series of both the March and

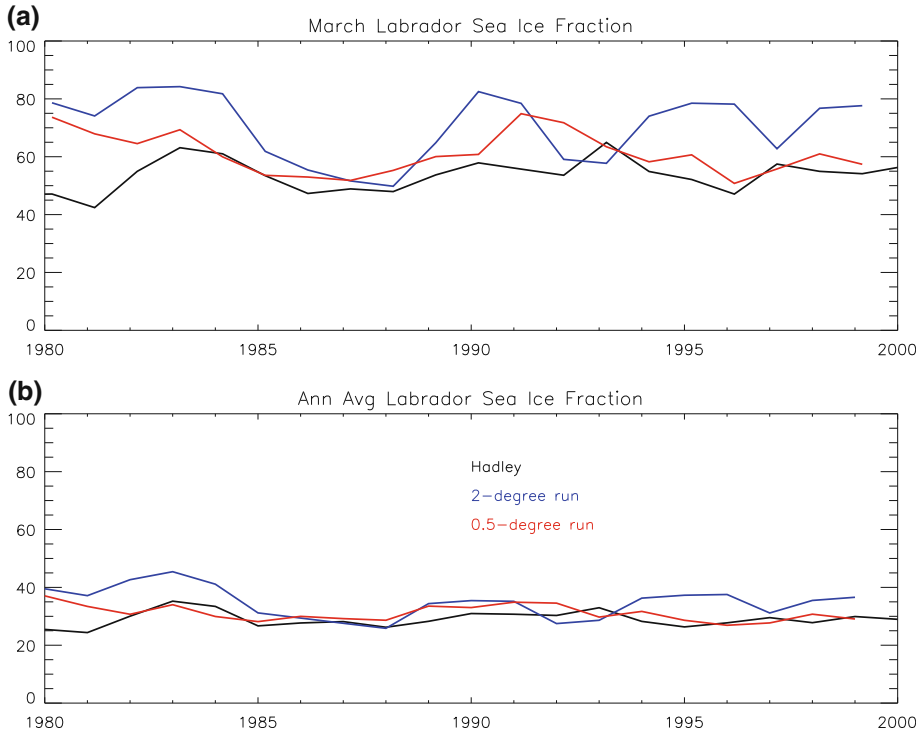

Fig. 15 Spatially-averaged Labrador Sea ice fraction expressed as a percentage between 1980 and 2000 from the 2° and 0.5° runs and observations (HadISST) for (**a**) March value, and (**b**) annual mean value

annual average Labrador Sea sea ice fraction (defined over a latitude–longitude box covering the Labrador Sea from Canada to Greenland) over the period 1980–2000 from the two runs and the HadISST observations (Rayner et al. 2003). Both the mean ice extent and the amplitude of the annual cycle are improved in the Labrador Sea in the 0.5° run. In addition, there is considerable decadal variability in the March sea ice extent in the observations, and its amplitude is captured better in the 0.5° run; the decadal amplitude is too large in the 2° run. Finally, it should be noted that both runs have very little ice in the Labrador Sea in September. This is a big improvement over the CCSM 3, which had much too extensive sea ice in the Labrador Sea. However, both the CCSM 3.5 runs have too much sea ice to the northeast of Iceland, which is a degradation compared to the CCSM 3 simulation.

The Antarctic sea ice simulations are comparable in the two runs, and there are no obvious improvements in the higher resolution 0.5° run. Again, the CCSM 3.5 Antarctic sea ice simulations are considerably improved over those obtained using the CCSM 3, with much reduced sea ice extent in the South Atlantic Ocean sector.

4 Conclusions and discussion

The main conclusion from this study is that there are considerable improvements in the climate of the 0.5° run of the CCSM 3.5 compared to the 2° run. The most significant is the reduction by more than 60% of the SST biases in the major upwelling regions, including the West Coast of the USA. There are improved precipitation patterns over North America, mostly due to the better resolved orography, and this leads to better river flows in a number of North American rivers. There are also improvements in the summer Asian monsoon and eastern tropical Pacific precipitation. The atmospheric circulation in the Arctic also improves, which leads to an improved regional sea ice thickness distribution in the Arctic Ocean.

Many of the improvements at 0.5° resolution documented above are due to the better interaction of the surface atmospheric flow with orography and better resolution of the atmospheric baroclinic eddies. Thus, we confidently expect that the improvements will also occur when the decadal projections and forecasts are done with the CCSM 4, rather than the CCSM 3.5 used in this study. However, increased resolution is not a panacea to eliminate all biases; as mentioned above, important biases such as the double-ITCZ in the western Pacific Ocean and the large SST error due to the incorrect Gulf Stream path in the North Atlantic are not improved at all in the 0.5° run. Biases remain in all components in the 0.5° run, which require further work and parameterization improvements to address them.

Finally, we note that the projected future climates over the USA between 2020 and 2030 in the 2° and 0.5° runs have significant differences. The largest difference occurs over the very northeast USA, where both the mean temperature and the projected temperature change differ in the two runs. As mentioned previously, the likely cause of the differences is the different strength of the baroclinic eddies

and position of the northern hemisphere jet stream in the two runs. We presume that the 0.5° run provides a better simulation of these features, but it is difficult to be absolutely certain. The reason is that we have rather little experience running the CAM 3.5 at 0.5° resolution, and it has not been as finely tuned in it's parameter values as the 2° version. This is one reason why we have not documented these differences late in the two climate projections in this paper. The other reason is that we are not sure whether the projected USA climate differences are smaller than the variability expected in an ensemble of climate projections using these two model versions. We cannot determine this at present, because there is only one projection each using the two model resolutions. An assessment of this question will have to wait until a larger ensemble of decadal projections and forecasts are performed using the CCSM 4.

Acknowledgments The National Center for Atmospheric Research is sponsored by the National Science Foundation. The 0.5° simulation was run on the "Franklin" supercomputer at the National Energy Research Scientific Computing Center of the Department of Energy's Lawrence Berkeley National Laboratory.

References

Bala G et al (2008) Evaluation of a CCSM3 simulation with a finite volume dynamical core for the atmosphere at 1° latitude by 1.25° longitude resolution. J Clim 21:1467–1486. doi:10.1175/2007JCLI2060.1

Brankovic C, Gregory D (2001) Impact of horizontal resolution on seasonal integrations. Clim Dyn 18:123–143. doi:10.1007/s003820100165

Branstetter ML, Erickson DJ (2003) Continental runoff dynamics in the Community Climate System Model (CCSM2) control simulation. J Geophys Res 108. doi:10.1029/2003JD003212

Briegleb BP, Light B (2007) A Delta-Eddington multiple scattering parameterization for solar radiation in the sea ice component of the Community Climate System Model. NCAR/TN-472+STR, 100 pp

Collins WD et al (2006) The community climate system model version 3 (CCSM3). J Clim 19:2122–2143. doi:10.1175/JCLI3761.1

Dai A, Trenberth KE (2002) Estimates of freshwater discharge from continents: latitudinal and seasonal variations. J Hydrometeorol 3:660–687. doi:10.1175/1525-7541(2002)003<0660:EOFDFC>2.0.CO;2

Danabasoglu G, Marshall J (2007) Effects of vertical variations of thickness diffusivity in an ocean general circulation model. Ocean Model 18:122–141. doi:10.1016/j.ocemod.2007.03.006

Danabasoglu G, Ferrari R, McWilliams JC (2008) Sensitivity of an ocean general circulation model to a parameterization of near-surface eddy fluxes. J Clim 21:1192–1208. doi:10.1175/2007JCLI1508.1

Guilyardi E et al (2004) Representing El Nino in coupled ocean/atmosphere GCMs: the dominant role of the atmospheric component. J Clim 17:4623–4629. doi:10.1175/JCLI-3260.1

Hack JJ, Caron JM, Danabasoglu G, Oleson KW, Bitz C, Truesdale JE (2006) CCSM–CAM3 climate simulation sensitivity to changes in horizontal resolution. J Clim 19:2267–2289. doi:10.1175/JCLI3764.1

Jochum M, Danabasoglu G, Holland MM, Kwon YO, Large WG (2008) Ocean viscosity and climate. J Geophys Res 113. doi:10.1029/2007JC004515

Keenlyside NS, Latif M, Jungclaus J, Kornblueh L, Roeckner E (2008) Advancing decadal-scale climate prediction in the North Atlantic sector. Nature 453:84–88. doi:10.1038/nature06921

Kobayashi C, Sugi M (2004) Impact of horizontal resolution on the simulation of the Asian summer monsoon and tropical cyclones in the JMA global model. Clim Dyn 23:165–176. doi:10.1007/s00382-004-0427-8

Large WG, Danabasoglu G (2006) Attribution and impacts of upper-ocean biases in CCSM3. J Clim 19:2325–2346. doi:10.1175/JCLI3740.1

Levitus S, Boyer T, Conkwright M, Johnson D, O'Brien T, Antonov J, Stephens C, Gelfeld R (1998) Introduction, vol 1. World Ocean Database 1998, NOAA Atlas NESDIS 18, 346 pp

Lin SJ (2004) A "Vertically Lagrangian" finite-volume dynamical core for global models. Mon Weather Rev 132:2293–2307. doi:10.1175/1520-0493(2004)132<2293:AVLFDC>2.0.CO;2

May W, Roeckner E (2001) A time-slice experiment with the ECHAM4 AGCM at high resolution: the impact of horizontal resolution on annual mean climate change. Clim Dyn 17:407–420. doi:10.1007/s003820000112

Navarra A et al (2008) Atmospheric horizontal resolution affects tropical climate variability in coupled models. J Clim 21:730–750. doi:10.1175/2007JCLI1406.1

Neale RB, Richter JH, Jochum M (2008) The impact of convection on ENSO: from a delayed oscillator to a series of events. J Clim 21:5904–5924. doi:10.1175/2008JCLI2244.1

Oleson KW et al (2008) Improvements to the Community Land Model and their impact on the hydrological cycle. J Geophys Res 113:G01021. doi:10.1029/2007JG000563

Pope V, Stratton R (2002) The processes governing horizontal resolution sensitivity in a climate model. Clim Dyn 19:211–236. doi:10.1007/s00382-001-0222-8

Rayner NA, Parker DE, Horton EB, Folland CK, Alexander LV, Rowell DP, Kent EC, Kaplan A (2003) Global analyses of sea surface temperature, sea ice, and night marine air temperature since the late nineteenth century. J Geophys Res 108:4407. doi:10.1029/2002JD002670

Richter JH, Rasch PJ (2008) Effects of convective momentum transport on the atmospheric circulation in the Community Atmosphere Model, version 3. J Clim 21:1487–1499. doi:10.1175/2007JCLI1789.1

Smith TM, Reynolds RW (1998) A high-resolution global sea surface temperature climatology for the 1961–90 base period. J Clim 11:3320–3323. doi:10.1175/1520-0442(1998)011<3320:AHRGSS>2.0.CO;2

Smith DM, Cusack S, Colman AW, Folland CK, Harris GR, Murphy JM (2007) Improved surface temperature prediction for the coming decade from a global climate model. Science 317:796–799. doi:10.1126/science.1139540

Steele M, Morley R, Ermold W (2001) PHC: a global ocean hydrography with a high-quality Arctic Ocean. J Clim 12:2079–2087. doi:10.1175/1520-0442(2001)014<2079:PAGOHW>2.0.CO;2

Stockli R, Lawrence DM, Niu GY, Oleson KW, Thornton PE, Yang ZL, Bonan GB, Denning AS, Running SW (2008) Use of FLUXNET in the Community Land Model development. J Geophys Res 113:G01025. doi:10.1029/2007JG000562

Williamson DL (2008) Equivalent finite volume and spectral transform horizontal resolutions established from aqua-planet simulations. Tellus 60:839–847. doi:10.1111/j.1600-0870.2008.00340.x

Willmott CJ, Matsuura K (2001) Terrestrial air temperature and precipitation: monthly and annual time series (1950–1999), version 3.02. Center for Climate Research, Department of Geography, University of Delaware, Newark